

Experimental power spectral density analysis for mid- to high-spatial frequency surface error control

JAVIER DEL HOYO,^{1,2} HEEJOO CHOI,¹ JAMES H. BURGE,^{1,3} GEON-HEE KIM,⁴ AND DAE WOOK KIM^{1,3,*}

¹College of Optical Sciences, University of Arizona, Tucson, Arizona 85721, USA

²NASA Goddard Space Flight Center, Greenbelt, Maryland 20771, USA

³Steward Observatory, University of Arizona, Tucson, Arizona 85721, USA

⁴Ultra-Precision Engineering Laboratory, Korea Basic Science Institute, Daejeon, South Korea

*Corresponding author: letter2dwk@hotmail.com

Received 2 March 2017; revised 20 May 2017; accepted 24 May 2017; posted 26 May 2017 (Doc. ID 287787); published 19 June 2017

The control of surface errors as a function of spatial frequency is critical during the fabrication of modern optical systems. A large-scale surface figure error is controlled by a guided removal process, such as computer-controlled optical surfacing. Smaller-scale surface errors are controlled by polishing process parameters. Surface errors of only a few millimeters may degrade the performance of an optical system, causing background noise from scattered light and reducing imaging contrast for large optical systems. Conventionally, the microsurface roughness is often given by the root mean square at a high spatial frequency range, with errors within a 0.5×0.5 mm local surface map with 500×500 pixels. This surface specification is not adequate to fully describe the characteristics for advanced optical systems. The process for controlling and minimizing mid- to high-spatial frequency surface errors with periods of up to $\sim 2\text{--}3$ mm was investigated for many optical fabrication conditions using the measured surface power spectral density (PSD) of a finished Zerodur optical surface. Then, the surface PSD was systematically related to various fabrication process parameters, such as the grinding methods, polishing interface materials, and polishing compounds. The retraceable experimental polishing conditions and processes used to produce an optimal optical surface PSD are presented. © 2017 Optical Society of America

OCIS codes: (220.0220) Optical design and fabrication; (220.4610) Optical fabrication; (220.5450) Polishing.

<https://doi.org/10.1364/AO.56.005258>

1. INTRODUCTION

The control and minimization of mid- to high-spatial frequency errors is highly desired in advanced precision optical systems. Surface errors not only affect the sharpness of the image, but also produce unwanted noise caused by light scatter in the system. Scatter reduces the core brightness of the point spread function as well as the encircled energy of an optical system. Systems with short wavelength applications are particularly affected because the total integrated scatter is inversely proportional to the square of the system wavelength [1,2].

The surface figure and finish are conventionally specified by root mean square (RMS) errors over a respective low- and high-spatial frequency bandwidth. Surface figure errors are usually measured with full- or sub-aperture phase shifting interferometry, but a high magnifying power interference objective is required to measure the surface finish. The RMS surface error specifications are sufficient for most commercial-grade optical components, but advanced precision optical systems often require a structure function or a power spectral density (PSD)

surface specification as a function of the spatial frequencies [3]. The surface specification is also given by the optical surface scattering performance in terms of the bidirectional reflectance distribution function (BRDF), which can be converted to the PSD function using the Rayleigh–Rice formula for super-smooth surfaces [1,2].

Smoothing experiments using different polishing processes to control the RMS surface roughness value have previously been reported [4–14]. Most have focused on measurements within an area of ≤ 1 mm², and have only compared RMS surface roughness values (the collapsed or integrated information of the fundamental PSD functions) for different methods. Various characterization approaches have been practical and useful for guiding various polishing processes for relevant cases, but they can be significantly improved by investigating a broader range of PSD values for more general and controlled fabrication conditions. In addition, as the final surface quality is affected by many external factors (e.g., optics shop temperature and air cleanliness, pitch type and age, etc.) that are not

practical to control, it is difficult to perform an objective comparison between separately reported experimental results.

A systematically controlled and statistically analyzed large set of experimental results (from a single source instead of multiple sources) enables an unbiased and retraceable comparison between different polishing processes—one of the most critical, yet omitted, pieces of information needed to plan and optimize a fabrication project. The experiments and measurements presented in this study were executed and produced using common fabrication machines, metrology equipment, and analysis software. Furthermore, an understanding of all of the details of the final surface PSD covering the mid- to high-spatial frequency bandwidths is essential for systematically and efficiently obtaining a super-smooth surface.

We acknowledge that the scope of the presented investigation does not reach out to the far low boundary of the mid-spatial frequency range (e.g., 10–50-mm-period tool-mark ripples from a computer-controlled dwell-time figuring run). This research is focused on the features much smaller than the tool size, so that the observed and investigated features are independent of the figuring process or tool misfit (e.g., freeform fabrication case). Thus, the local surface characteristics are isotropic and uncorrelated to each other.

Low-spatial frequency errors are effectively controlled with optimized computer-controlled optical surfacing techniques, requiring a variation in the tool dwell time and/or tool stroke speed to obtain the desired surface removal distribution [6]. Conversely, mid- to high-spatial frequency errors are smaller than the tool size and depend more on the process parameters, such as polishing interface material, polishing compound, and total polishing time.

Some of the most common polishing parameters have been examined in a large study of controlled experiments conducted on a Zerodur surface. Zerodur was chosen as the workpiece material owing to its outstanding physical properties, nearly zero coefficient of thermal expansion, and many practical applications [15–17]. (We acknowledge that the presented results may vary when using different glass types. The present study focused on providing a wide range of experimental data for comparing different polishing parameters on the fixed substrate type). During each experiment, one parameter influencing the surface PSD was varied while the other parameters were kept constant so the effect of each variable is well observed in terms of the PSD. A theoretical background for the polishing process is presented in Section 2. The experimental parameters for the grinding and polishing phases are presented in Section 3, while the results and concluding remarks are discussed in Sections 4 and 5.

2. PROCESS PARAMETERS FOR OPTICAL FABRICATION

A. Preston's Basic Parameters

The material removal process during optical fabrication is described by Preston's equation [18],

$$\Delta z(x, y) = \kappa \cdot P(x, y) \cdot V(x, y) \cdot \Delta t(x, y), \quad (1)$$

where x and y are local coordinates on the workpiece surface, $\Delta z(x, y)$ is the integrated material removed, κ is Preston's

constant defining the removal rate, $P(x, y)$ is the local polishing pressure, $V(x, y)$ represents the relative speed between polishing tool and workpiece, and $\Delta t(x, y)$ is the dwell time of the polishing tool. To acquire reliable, practical, and reproducible experimental data, these basic parameters P , V , and Δt were controlled throughout the experiments conducted, as described in Sections 3 and 4.

B. Polishing Interface Materials

The polishing interface material touching the workpiece surface plays an important role in obtaining a superb surface finish. This is primarily dependent on the polishing material's compliance and material properties, such as viscosity of the pitch [19]. Various polyurethane pads such as LP-66 are also popular polishing interface materials and produce different characteristic surface finishes compared to pitch [6].

Polishing with pitch is one of the common methods for obtaining a super-smooth surface. Pitch's property is often described using viscosity, with the measurement of a material's resistance to deform given as the shear stress divided by the strain rate,

$$\eta = \frac{F/A}{v/l}. \quad (2)$$

η is the material viscosity, F is the applied shear force, A is the area in contact with the fluid, v is the velocity of the shear flow, and l is the thickness of the fluid. Viscosity is exponentially dependent on temperature, given as [20–22]

$$\eta = \eta_0 e^{Q/RT}, \quad (3)$$

where η_0 is a constant dependent on the material, Q is the molar activation energy for viscous flow, R is the universal molar gas constant, and T is the temperature. In order to maintain consistent removal and surface finish on the polished surface, these properties of pitch have to be effectively controlled.

In practice, a pitch's characteristic can be classified with the indentation test [19]. The procedure involves a silicon mold, a spring-loaded dial indicator setup, and a pitch sample. As pitch is melted to make a pitch tool, a portion of the pitch is replicated in a silicon mold. After reaching room temperature, the molded pitch sample puck is tested with a spring-loaded dial indicator on an aluminum stand. The distance that the dial indicator tip indents the pitch sample as a function of time is measured, and the results are averaged for each sample. In order to present repeatable and objective experimental data, the pitch's indentation rate (with a consistent temperature) was measured using a 6-mm-diameter ball with a 0.84-kg load and reported in this study.

C. Polishing Compounds

The polishing process consists of chemical [4,22–24] and mechanical [22,23,25] interactions between the polishing material, compound abrasives, and glass, all of which affect the surface finish. The particles in the polishing compound embed the material used to polish the workpiece, depending on the material's ductility. Brown and Cook suggested a model based on spherical particles in the polishing compound elastically indenting the glass surface and gouging a path, which predicted a surface finish expressed as [22]

$$R_s = \frac{3}{4} \phi \left(\frac{P}{2kE} \right)^{2/3}, \quad (4)$$

where the surface roughness, which is the penetration depth of the particle into the surface, is R_s ; ϕ is the polishing compound mean particle diameter; P is the pressure of the particles exerted on the glass surface; E is the Young's modulus of the workpiece material; and k is the particle concentration. When polishing abrasives embed the whole polishing material area in contact with the workpiece, the particles in the polishing compound carry the load on the surface being polished, and smaller particle diameters result in smaller indentation depths, reducing the surface roughness. In addition, Suratwala *et al.* reported a significant result relating the particle size distribution and the optical surface quality resulting from subsurface damage or scratches [26]. Izumitani describes the creation of a gel layer, chemically formed by the water and silica glass when it is removed by the interaction of the glass surface and the abrasive particles [23]. Cumbo hypothesized that the polishing process is dependent on the pH of the slurry to prevent agglomeration of particles in the compound, which increases the surface roughness [4]. Kaller believed that lattice defects in the polishing abrasives assisted in gripping the glass for material removal [24]. In practice, however, the actual surface PSD function and RMS surface roughness depend on an entangled effect of both chemical and mechanical interactions. The gap between the theories and real outcomes is filled by acquiring and analyzing experimental data, which delivers the core value of the presented database results. The final PSDs for various polishing compound cases were experimentally measured and compared, and are presented in Section 4.

3. EXPERIMENT DESIGN AND DATA PROCESSING

A. Rough-to-Fine Grinding for Workpiece Preparation

The substrates used were 250-mm-diameter Zerodur workpieces. The surfaces were made flat using cup wheel generation and rough-to-fine ground with a tile grinding tool using aluminum oxide loose abrasives. The parameters used during the grinding procedure for the desired removal of material are summarized in Table 1. They were developed using the same tool pressure and spindle speed, with the exception of when comparing the PSD as a function of polishing time after ending two different loose abrasive fine grinding stages with the 5- and 9- μm grits. The systematic grinding phase (Common Phase) removes ambiguities in the results, so the resulting PSD depends solely on the polishing phase parameters discussed in Section 3.B.

An attractive option for some cases is bound abrasive grinding with Trizact pads, which is known for removing material at a faster rate while leaving less subsurface damage than loose abrasive grinding [27]. In addition to comparing the two different grit size methods listed in Table 1, the PSD was examined after ending with 9- μm aluminum oxide loose abrasive and compared to the 9- μm diamond bound abrasive process.

Some Zerodur substrates were rough-to-fine ground using Trizact diamond pads. The same procedure was applied as for

Table 1. Aluminum Oxide Loose Abrasive Grinding Parameters

	Grit Size (μm)	Removal Depth (μm)	Pressure (PSI)	Spindle Speed (RPM)
Common Phase	40	~100	0.25	60
	25	~75	0.25	60
	12	~50	0.25	60
9- μm Grit Finish Case	9	~40	0.25	60
5- μm Grit Finish Case	5	~25	0.25	60

the loose abrasive grinding: removing material from larger to smaller grit size to remove the scratch depth, and/or subsurface damage from the prior grit size [27]. The specific grinding parameters used for this lapping stage are presented in Table 2.

B. Experimental Polishing Process Design

After the grinding phase, the Zerodur substrates were polished using full-size laps (300 mm in diameter) with various polishing parameters as discussed in Section 2, while the optical surface was measured after each trial and analyzed. A fixed 0.3-psi polishing pressure with 50-rpm substrate spindle speed was set and kept constant for all experiments. There were five experimental categories (Studies 1–5) investigated, with the parameters summarized in Table 3.

Experimental polishing configurations were carefully designed and controlled to minimize ambiguous factors in the results. The pitch lap was always pressed on the workpiece for a sufficient amount of time to remove any ambiguity due to tool misfit. Equal width channels were cut into the pitch lap to maintain the same pitch facet sizes and compliance as the pitch flowed. The charging of the pitch lap was monitored to assure only the charged areas made contact with the surface being polished. The relative density of polishing compound to water was fixed at 17%–20% using a hydrometer and a graduated cylinder. All the LP-66 polyurethane pads were initially conditioned on a dummy optical surface to smooth the rough surface of the new pads [6].

The following investigations are reported: the accumulated polishing time required to achieve the final surface quality for the final PSD using different fine grinding approaches (Studies 1 and 2); the PSD difference and polishing efficiency between the polishing interface materials and compounds (Studies 3 and 4); and the improvement in the PSD via the Aqua polishing technique utilizing distilled water (Study 5).

Table 2. Grinding Parameters: Loose Versus Bound Abrasive Approach

	Grit Size (μm)	Removal Depth (μm)	Pressure (PSI)	Spindle Speed (RPM)
Loose Abrasives (Aluminum Oxide)	25	~75	0.3	50
	12	~45	0.3	50
	9	~25	0.3	50
Bound Abrasives (Trizact)	20	~70	0.3	50
	9	~35	0.3	50

Table 3. Polishing Experimental Configurations

	Study 1	Study 2	Study 3	Study 4	Study 5
Fine grind finish	5-μm/9-μm loose abrasives	9-μm bound/loose abrasives	5- μ m loose abrasives	5- μ m loose abrasives	5- μ m loose abrasives
Polishing interface material	CP (Conventional Pitch) #64	SP (Synthetic Pitch) #64	CP #73/#64/#55 SP #64/#55	CP#64 SP #64 LP-66 (Polyurethane pad)	CP #55 SP #55
Polishing compound	Opaline	Rhodite-906	Rhodite-906	Opaline Zirox-K Iron Oxide Rhodite-906	Rhodite-906 Distilled water^a
Polishing time	1–8 h	1–8 h	Until converging to a final PSD (\sim 3 h)	Until converging to a final PSD	Until converging to a final PSD (\sim 3 h)
Results in	Section 4.A	Section 4.B	Section 4.C	Section 4.D	Section 4.E

^aNo polishing compound but distilled water was used during the Aqua polishing process.

Note: **Bold** parts represent the key parameters that have been investigated and compared during each study.

C. Surface PSD Measurement

The Micro Finish Topographer (MFT) in Fig. 1 was used as the *in situ* measurement device [28], having the ability to measure mid- to high-spatial frequency errors as shown in Table 4. In order to present statistically meaningful results, considering the isotropic and uncorrelated local surface shapes, 15 randomly distributed MFT measurements were sampled over the workpiece area and averaged after each experimental polishing run.

The MFT instrument was calibrated by averaging the sampled reference surface measurements and subtracting the resulting fixed system calibration map from each surface measurement [29].

The two-dimensional PSD_{2d} can be computed from the MFT surface height measurements $z(x, y)$ by [2]

$$\text{PSD}_{2d}(f_x, f_y) = \lim_{\text{Area} \rightarrow \infty} \frac{1}{\text{Area}} |\mathcal{FF}[z(x, y)]|^2, \quad (5)$$

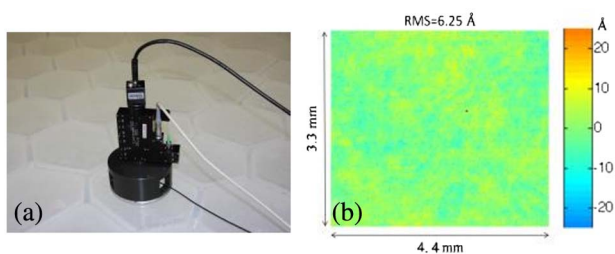


Fig. 1. (a) MFT on an optical surface measuring the local surface shape using an interference microscope objective. (b) Typical surface measurement data collected from the $2.5\times$ interference objective.

Table 4. MFT Specifications

	Specification	
Camera detector resolution	1599 \times 1199 pixels	
Microscope objective magnification	2.5 \times	10 \times
Object space pixel size	2.76 μ m	0.69 μ m
Spatial field of view	4.4 \times 3.3 mm	1.1 \times 0.8 mm

where FF is the two-dimensional Fourier transform. The PSD_{2d} can then be azimuthally averaged by assuming the statistical surface height distribution is isotropic, resulting in a radial spatial frequency analysis $f_\rho = \sqrt{f_x^2 + f_y^2}$. The averaged PSD analysis as a function of radial spatial frequency is discussed in Section 4.

D. Band-Limited RMS Surface Roughness Versus Time

The RMS surface roughness progression as a function of time, $\varepsilon(t)$, can be given as [30]

$$\varepsilon(t) = \varepsilon_0 + (\varepsilon_{\text{int}} - \varepsilon_0)e^{-k't}, \quad (6)$$

where ε_{int} is the initial RMS surface roughness, k' is a constant based on the polishing process parameters with units of inverse time, and ε_0 is the final converged RMS surface roughness.

One can deduce these variables from the PSD_{2d} map and determine the most efficient polishing process. The band-limited RMS is determined by integrating and processing the PSD_{2d} map over a spatial frequency bandwidth. An example case showing the resulting band-limited RMS surface roughness plotted as a function of time is shown in Fig. 2. The data is then fit to an exponential decay model in

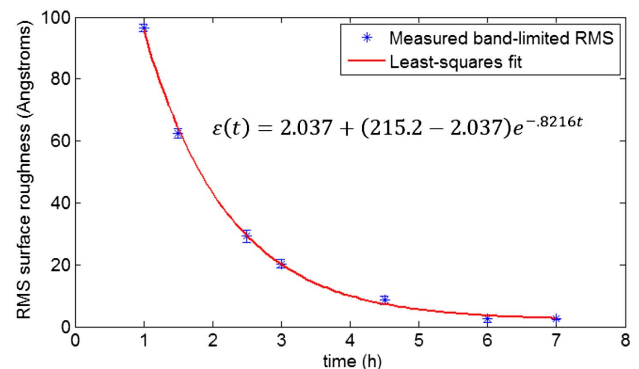


Fig. 2. Band-limited RMS surface roughness versus time data for polishing after bound abrasive grinding. The data is fit to Eq. (6) using the least squares solution. (Error bar, $\pm\sigma$; RMS bandwidth, 0.0004–0.1 μm^{-1}).

Eq. (6) using the method of least squares, and the values of the unknown variables are attained.

Note: All the experimental data, such as RMS and PSD values, have been statistically processed. Most plots in Section 4 show error bars of $\pm\sigma$, representing the standard deviation of the data points.

4. EXPERIMENTAL DATA ANALYSIS AND DISCUSSIONS

A. Study 1: PSD Evolution After 9- μm Versus 5- μm Loose Abrasive Grinding

The change in the RMS surface roughness and PSD as a function of the polishing time was monitored after fine grinding and compared for the 9- μm and 5- μm aluminum oxide loose abrasives. This was used to investigate the effect of the last fine grinding grit size on the surface error reduction during the following polishing process. The spatial frequency error reduction was monitored as a function of time, indicating which surface spatial frequencies become “smoothed” the fastest to a final PSD magnitude. The band-limited RMS surface roughness was plotted as a function of time and fit to Eq. (6). These variables are listed in Table 6 of Appendix A.

Both fine-ground Zerodur substrates were polished periodically using a conventional pitch (#64) tool with an Opaline polishing compound (more specific parameters are listed under Table 3, Study 1), while the surface map was measured with the MFT following every polishing run. The experiments were conducted until the analyzed surface PSD converged to a single curve without improvements, which occurred after ~ 5 h of polishing following the 5- μm fine grind, and ~ 6.5 h following the 9- μm fine grind, as shown in Fig. 3.

The lower-spatial frequency errors of less than $4 \times 10^{-3} \mu\text{m}^{-1}$ steadily decreased until they remained unchanged regardless of more polishing time under the same polishing conditions. The higher-frequency errors were predominant in both experiments and took longer to smooth and plateau. The rate for the PSD to converge to a single curve was faster after the 5- μm fine grind than for the 9- μm fine grind, when comparing the PSD progression as a function of time, as seen in Fig. 3.

These results are further verified in Fig. 4, where the surface error RMS decreases at a faster rate for the 5- μm grit size case. The final surface PSD for both cases converges to the same result, and the RMS surface roughness steadily approaches a

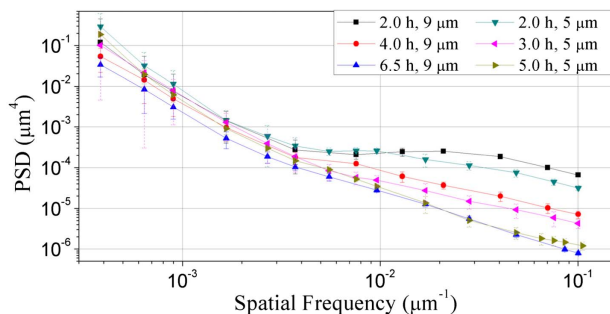


Fig. 3. Azimuthally averaged PSD as measured at given polishing times with conventional pitch #64 and Opaline, following a 9- μm fine grind and 5- μm fine grind. (Error bar, $\pm\sigma$).

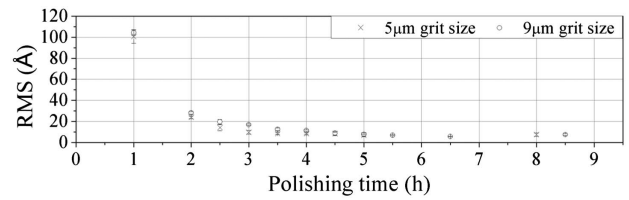


Fig. 4. Surface roughness RMS of a Zerodur surface as a function of polishing time after 5- μm versus 9- μm fine grind. (Error bar, $\pm\sigma$; RMS bandwidth, 0.0004–0.1 μm^{-1}).

similar constant value of $\sim 7 \text{ \AA}$. The results confirm that i) the final grinding grit size affects the polishing time needed to achieve the final PSD surface quality, and ii) a similar final PSD (not just RMS) after different fine grinding finishes is achievable at the cost of a longer polishing time.

In practice, it may be advantageous for a given project, considering other factors such as subsurface damage, removal rate, available metrology systems, and other costs (for each fabrication phase) to reach an optimal PSD finish.

B. Study 2: Final PSD After Bound Versus Loose Abrasive Fine Grinding

The change in the PSD (Fig. 5) and RMS surface roughness (Fig. 6) as a function of polishing time was analyzed following a 9- μm aluminum oxide loose abrasive fine grind and a 9- μm diamond bound abrasive fine grind. After the grinding phases, each substrate was polished with a charged #64 synthetic pitch tool using the Rhodite-906 polishing compound. Surface measurements were incrementally taken every 0.5–1 h of polishing. The polishing parameters used for this comparison of loose and bound abrasives are listed in Table 3, Study 2. The RMS

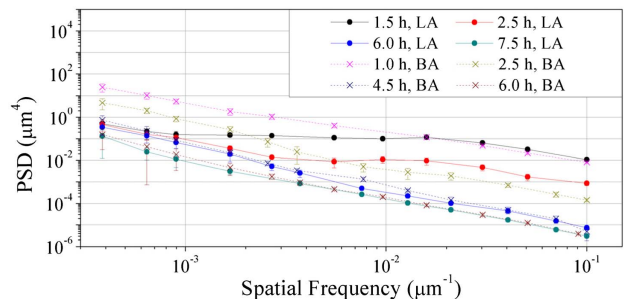


Fig. 5. Azimuthally averaged PSD measured during 8 h of polishing with a synthetic pitch tool using Rhodite-906, following a 9- μm aluminum oxide loose abrasive (LA) fine grind versus a 9- μm Trizact diamond bound abrasive (BA) fine grind. (Error bar, $\pm\sigma$).

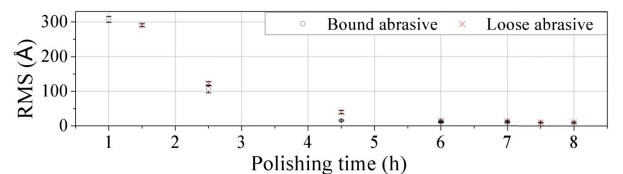


Fig. 6. Surface roughness RMS convergence after a 9- μm grit size loose versus bound abrasive grind on a Zerodur surface. (Error bar, $\pm\sigma$; RMS bandwidth, 0.0004–0.1 μm^{-1}).

surface roughness was also plotted as a function of time and fit to Eq. (6). The curve fit variables are listed in Table 6 of Appendix A.

Comparing the PSD progression shown in Fig. 5, as also seen in prior results from Figs. 3 and 4, the higher-frequency errors take the longest time to polish and reach a converging PSD after a loose abrasive grind. For the bound abrasive case, the overall PSD magnitude, in the spatial frequency bandwidth provided, evenly decreases with polishing time until reaching a converging PSD in 6 h, while the substrate ground with loose abrasives took 7.5 h. Both substrates, however, converged towards the same PSD function.

The RMS convergence is shown in Fig. 6. After 2.5 h of polishing, the substrate that was ground with loose abrasives had an RMS surface roughness of 122 Å, while that of the substrate ground with bound abrasives was 107 Å.

The RMS surface roughness quickly decreases within the first 4–5 h of polishing and then steadily decreases until it reaches a final RMS surface roughness value of ~ 10 Å RMS for both cases. The RMS surface roughness value decreased for the substrate ground by bound abrasives and it finalized at a faster rate.

C. Study 3: Final PSD for Conventional Versus Synthetic Pitch

Conventional and synthetic pitches come in different grades: #73, #64, and #55, where the larger numbers usually represent a more viscous pitch. The indentation rate for the synthetic and conventional pitches was measured as described in Section 2.B (shown in Fig. 7) to achieve a quantitative characterization for every type of pitch used in the experiments. Three Zerodur surfaces were polished with #73, #64, and #55 conventional pitches, while two were polished with #64 and #55 synthetic pitches. The detailed polishing parameters for each substrate are shown in Table 3, Study 3.

The difference between the surface finish of conventional (CP) and synthetic (SP) pitches is compared in terms of the RMS surface finish, as shown in Fig. 7. The RMS surface roughness of the #73 conventional pitch (9.4 Å) is comparable to that of the #64 synthetic pitch (9.7 Å). The pitch with a higher indentation rate tends to result in lower RMS surface roughness values.

As shown in Fig. 8, the PSD magnitude at all frequencies was significantly lower for the softer (i.e., higher-indentation-rate) pitches. The conventional pitch produced the best results compared to the synthetic pitch; the #64 conventional pitch produced a better PSD than the #64 synthetic pitch, as the PSD of the #64 synthetic pitch is comparable to that of the

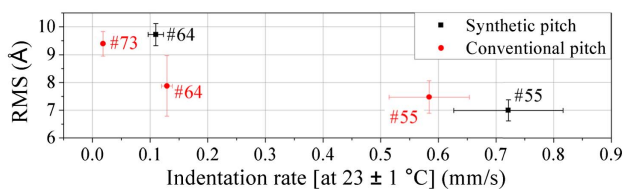


Fig. 7. Indentation rate of pitch material for pitch viscosity tester used in experiments at \log_{10} scale. (Error bar, $\pm\sigma$; RMS bandwidth, 0.0004–0.1 μm^{-1}).

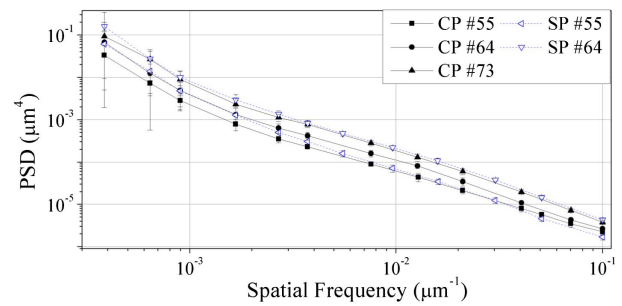


Fig. 8. Azimuthally averaged final PSD after polishing with #73, #64, and #55 conventional pitches (CP) and #64 and #55 synthetic pitches (SP). (Error bar, $\pm\sigma$).

#73 conventional pitch. The #55 synthetic pitch performed slightly better (i.e., lower PSD) at higher frequencies, while the #55 conventional pitch produced better results at lower frequencies of less than $1 \times 10^{-2} \mu\text{m}^{-1}$.

D. Study 4: PSD and Polishing Efficiency for Various Compounds and Interface Materials

The smoothing caused by various combinations of different polishing interface materials and compounds was examined. Polishing interfaces vary in properties from different pitch blends and polishing pads, so the interaction between particles in the polishing compound and the polishing material will cause a unique final PSD [31]. The polishing parameters of three materials (conventional pitch #64, synthetic pitch #64, and polyurethane pad LP-66) in various combinations with polishing compounds (Rhodite-906, Zirox-K, Opaline, and iron oxide) were investigated as summarized in Table 3, Study 4. (Note: Zirox-K was chosen to represent a zirconium-oxide-based polishing compound, while Rhodite-906 is one of the most popular cerium-oxide-based compounds.)

The resulting PSDs are given in Fig. 9. For the conventional pitch #64 in Fig. 9(a), Rhodite-906 had the best performance at lower spatial frequencies of the spectrum, while Opaline and iron oxide performed better at higher frequencies. Polishing with synthetic pitch produced results similar to those for the conventional pitch on the final PSD, as shown in Fig. 9(b), where iron oxide excelled at higher spatial frequencies, and the performances of Rhodite-906 and Zirox-K were comparable. Unlike the synthetic and conventional pitch, the final PSD using polyurethane pads always converged to similar results for different polishing compounds, as shown in Fig. 9(c). Based on these results, when polishing with pitch, the choice of polishing compound is critical when considering the surface finish PSD spectrum.

The performance of each polishing compound with each respective polishing interface material was also investigated by categorizing the results into different groups. As seen in Figs. 9(d) and 9(e), conventional pitch #64 outperformed both synthetic pitch #64 and polyurethane LP-66 materials when using Rhodite-906 and Zirox-K polishing compounds at most frequencies. However, when using iron oxide, both synthetic and conventional pitch #64 performed well, while still outperforming the polyurethane pad LP-66, as observed in Fig. 9(f).

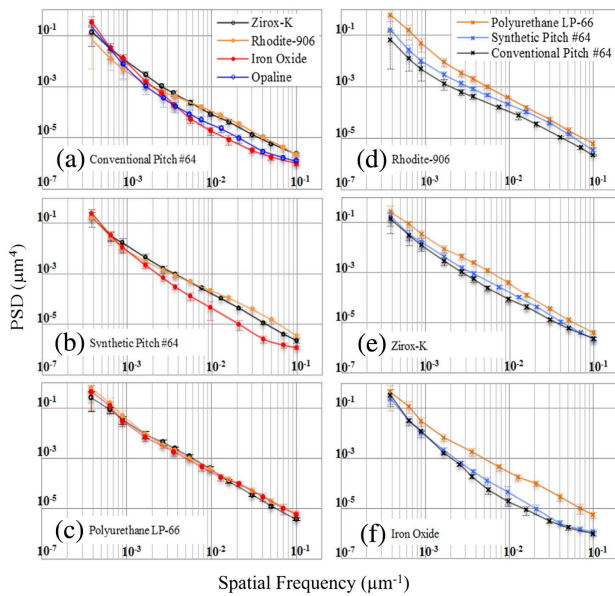


Fig. 9. Azimuthally averaged final PSD for Rhodite-906, Zirox-K, iron oxide, and Opaline polishing compounds used with (a) conventional pitch #64, (b) synthetic pitch #64, and (c) polyurethane LP-66, with all other parameters such as pressure, speed, tool size, etc., kept constant for each trial. PSD using the conventional pitch #64, synthetic pitch #64, and polyurethane LP-66 with (d) Rhodite-906, (e) Zirox-K, and (f) iron oxide polishing compounds, with all other parameters kept constant. (Error bar, $\pm\sigma$) Note: Graphs in (a), (b), and (c) and (d), (e), and (f) share the same data with different grouping.

The band-limited PSD was fitted using piecewise functions, and the variables are listed in Table 5 of Appendix A.

In general, with every polishing compound investigated, pitch performs better than a polyurethane pad in terms of RMS surface finish, as shown in Fig. 10(a). When using Rhodite-906, the average surface roughness for all repeated experiments using #64 conventional and synthetic pitches and polyurethane LP-66, is 7.6, 9.6, and 15.0 Å, respectively. Using iron oxide as the polishing compound produced similar results for #64 conventional and synthetic pitches at 8 Å and 7.3 Å RMS, respectively, while performing worse with polyurethane LP-66 at 14 Å. It is also noticeable that synthetic pitch tends to produce a smaller standard deviation than other materials, so synthetic pitch can lead to a more predictable surface finish.

The efficiency of each polishing configuration was also tested for various combinations. As can be seen in Fig. 10(b), Rhodite-906 performed most efficiently as it reached the final PSD and within 5 h. Opaline took nearly the same time as Rhodite-906, while Zirox-K performed least efficiently, requiring 6.5 h to acquire the final PSD. Comparing the polishing interface materials, the #64 conventional and synthetic pitch performed the best, requiring only 4–5 h of polishing with Rhodite-906 to converge to a final PSD. The polyurethane pad took almost twice as long as the pitch to reach the final PSD.

E. Study 5: PSD Improvement via Aqua Polishing Technique

The RMS surface roughness was analyzed for conventional and synthetic pitch and compared to the average particle size of each

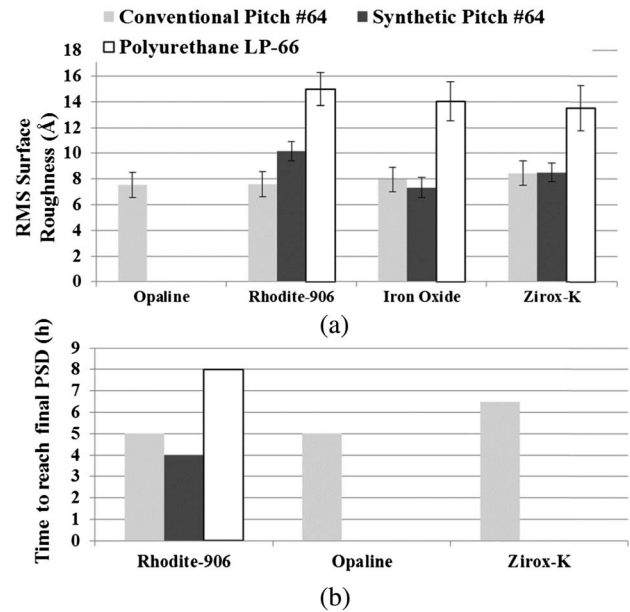


Fig. 10. (a) Final RMS surface roughness for Opaline, Rhodite-906, iron oxide, and Zirox-K polishing compounds with conventional pitch #64, synthetic pitch #64, and LP-66 polyurethane pad polishing interface materials. (b) Polishing time to reach the final PSD after 5- μm grit size loose abrasive fine grinding. (Error bar, $\pm\sigma$; RMS bandwidth, 0.0004–0.1 μm^{-1}).

polishing compound given by Universal Photonics [32]. There was a trend that the smaller polishing compound particle sizes produced a better RMS surface finish, as shown in Fig. 11.

Since polishing compound particle size affected surface finish, Study 5 investigated a compoundless approach—Aqua polishing—by comparing the surface finish between Rhodite-906 and distilled water. When a pitch lap becomes charged, the particles in the polishing compound become load bearing and polish the surface. The surface finish produced when charging a lap first and then replacing the polishing compound with distilled water was tested. The detailed experimental polishing parameters are presented in Table 3, Study 5.

As is seen in Fig. 12, about 3 h of Aqua polishing using a Rhodite-906 charged pitch lap significantly improves the surface finish as the PSD magnitude at all spatial frequencies decreased for both conventional and synthetic pitch case.

For the #55 conventional pitch, the finish went from 7.5 Å RMS when polishing with Rhodite-906 to 6.6 Å when polishing with distilled water, as shown in Fig. 13. There

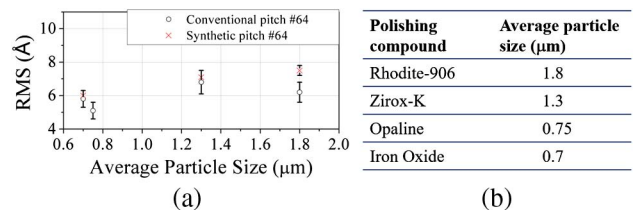


Fig. 11. (a) RMS surface roughness as a function of polishing compound particle size; (b) polishing compound with its respective particle size [32]. (Error bar, $\pm\sigma$; RMS bandwidth, 0.0004–0.1 μm^{-1}).

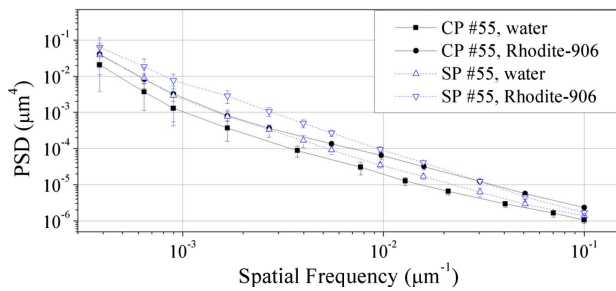


Fig. 12. Azimuthally averaged PSD when polishing with Rhodite-906 versus distilled water (i.e., Aqua polishing) using conventional pitch (CP) #55 and synthetic pitch (SP) #55. (Error bar, $\pm\sigma$).

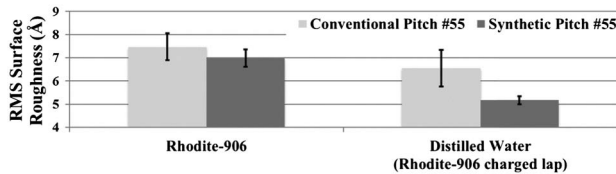


Fig. 13. RMS surface roughness of Zerodur surface when polishing with Rhodite-906 versus distilled water (i.e., Aqua polishing) on a #55 conventional pitch and a #55 synthetic pitch. (Error bar, $\pm\sigma$; RMS bandwidth, $0.0004\text{--}0.1\ \mu\text{m}^{-1}$).

was a marked difference in surface finish when polishing with the #55 synthetic pitch and water, where the surface finish went from 7 Å RMS with Rhodite-906, to 5.2 Å RMS after the Aqua polishing using distilled water. The Aqua polishing technique is suitable for use when the optical surface PSD requires the very best finishing refinements; however, this is at the expense of extra final polishing time.

5. CONCLUDING REMARKS

The final surface PSD covering the mid- to high-spatial frequency spectrum is highly dependent on the polishing parameters. The evolution of the PSD with the polishing time was compared to the grinding phase that the substrates had

incurred. It was verified that the polishing time to reach the final PSD depends on the polishing material and compound. In terms of the final PSD, polishing with conventional and synthetic pitch interfaces resulted in the best performance. The best-performing polishing compounds were Opaline and Rhodite-906 when using a conventional pitch, and iron oxide when using a synthetic pitch. Finally, Aqua polishing with distilled water improved the surface finish with a synthetic and conventional pitch (Rhodite-906-charged) lap.

Many of the most common and sought-after polishing parameters were extensively studied through more than 100 total experimental trials, and their respective effects on the surface PSD have been presented for working on a Zerodur surface. We acknowledge that the presented results may not be generalized for all optical polishing cases, as the actual polishing process depends on multiple and complicated factors. However, the experiments were carefully designed so that: (i) the configurations demonstrate a wide variety of representative cases (e.g., three of the most common polishing compound materials, i.e., cerium, zirconium, and iron oxide, were used); (ii) the suggested polishing parameters are available for most optical engineering shops; and (iii) the measured PSD data provide an invaluable experimental reference.

Also, there is a recent initiative in the optics manufacturing society to adapt machine learning or Artificial Intelligence (AI)-assisted mass manufacturing processes for high-precision optics [33]. Unfortunately, one of the technical challenges is the lack of sufficient and fully described archival data to educate/teach the machines. In addition to the theoretical models and optician’s knowledge, various experimental databases will be an essential component for the AI-assisted process developments.

It is worth mentioning that an intimate fit between the tool and workpiece is essential to obtain stable removal footprints (i.e., Tool Influence Function) and excellent surface smoothness. While a freeform conformable tool development itself is another active research area [6,30], this study assumes a good fit between the tool and workpiece by using a properly designed tool for a given aspheric/freeform manufacturing application.

In addition to the other theoretical references and limited scale data (such as the $10 \times 10\ \text{mm}$ glass sample results), the

Table 5. Piecewise PSD (μm^4) Linear Estimation as a Function ($\log_{10}(\text{PSD})=X \cdot \log_{10}(f) - Y$) of Frequency f (μm^{-1})

Polishing Compound	Interface Material	Spatial Frequency f (μm^{-1}) Range		
		X, Y		
Rhodite-906	CP	0.0004–0.0100	0.0100–0.0350	0.0350–0.1000
		–1.36, –6.68	–1.73, –7.35	–1.84, –7.50
	SP	–1.53, –6.78	–1.57, –6.80	–2.11, –7.57
		0.0004–0.0040	0.0040–0.1000	
Zirox-K	CP	–2.27, –8.78	–1.56, –7.23	
		–1.91, –7.61	–1.91, –7.61	
	SP	0.0004–0.0100	0.0100–0.0350	0.0350–0.1000
		–1.92, –8.35	–1.81, –8.06	–1.30, –7.32
Opaline	CP	0.0004–0.0030	0.0030–0.0300	0.0300–0.1000
		–2.99, –10.98	–1.77, –8.27	–0.95, –6.99
	SP	–2.87, –10.60	–1.98, –8.36	–0.90, –6.87
		–2.99, –10.98	–1.77, –8.27	–0.95, –6.99

Table 6. RMS Surface Irregularity Fit Constants at Three Equal Spatial Frequency f (μm^{-1}) Bandwidths (units: k' (h^{-1}), ϵ_0 (\AA), ϵ_{ini} (\AA))

Abrasive	Fit Const.	Spatial Frequency f (μm^{-1}) Range		
		0.0004–0.0336	0.0336–0.0668	0.0668–0.1000
5 μm , Loose ^a	k'	1.98	1.71	1.56
	ϵ_0	2.66	1.55	1.34
	ϵ_{ini}	184.00	199.70	128.30
9 μm , Loose ^a	k'	1.07	1.05	1.01
	ϵ_0	2.27	1.46	1.28
	ϵ_{ini}	54.39	73.49	54.70
9 μm , Bound ^b	k'	0.8272	0.8216	0.8424
	ϵ_0	5.98	2.04	0.93
	ϵ_{ini}	264.60	215.20	148.80
9 μm , Loose ^b	k'	1.01	0.93	0.93
	ϵ_0	6.62	2.91	2.05
	ϵ_{ini}	411.70	414.10	267.90

^aStudy 1 (Section 4.A, 9- μm versus 5- μm aluminum oxide loose abrasives, Conventional Pitch #64, Opaline polishing compound).

^bStudy 2 (Section 4.B, 9- μm aluminum oxide loose abrasive versus 9- μm diamond bound abrasive, Synthetic Pitch #64, Rhodite-906 polishing compound).

baseline is available to plan or optimize actual optical manufacturing processes, specifically those requiring very high-quality PSD specifications. Additionally, the PSD data for each polishing compound were fit to a linear piecewise function consisting of three equations for conventional and synthetic pitches, which can be found in Appendix A.

APPENDIX A

The final PSD data for each polishing compound case were fit to a linear piecewise function consisting of three equations for conventional and synthetic pitches. With this information, readers will be able to decide which polishing process to use based on the target optical surface PSD specification. The data for each polishing compound were incrementally fit to three distinct spatial frequency bandwidths for each polishing compound. The linear fit for each bandwidth was estimated using the least-squares solution. Table 5 below shows the piecewise function chosen for each polishing compound on synthetic and conventional pitches. The PSD and frequency data were converted to a \log_{10} scale to properly fit linear functions for each spatial frequency bandwidth.

As described in Section 3.D, the RMS surface roughness progression as a function of time can be expressed as an exponential decay. The data, when comparing RMS surface roughness as a function of time for the cases of polishing after using the loose and bound abrasive grinding methods, were fit to Eq. (6) at three equal spatial frequency bandwidths ranging from 0.0004 to 0.1 μm^{-1} . The variables extracted from the equation are listed in Table 6. (While this extra fitting data provides an efficient way to estimate a RMS value, please note that it is also limited by the number of fitting data points and residual error.)

Funding. Association of Universities for Research in Astronomy (AURA) (C22026SB).

Acknowledgment. We acknowledge that data from Sections 4.A and 4.D in this study was presented as a preliminary result in a previous conference paper [31]. This material is partly based on work performed for the Daniel K. Inouye Solar Telescope (DKIST). DKIST is managed by the National Solar Observatory, which is operated by the Association of Universities for Research in Astronomy Inc. under a cooperative agreement with the National Science Foundation. In addition, this material is based in part upon work performed for the “Post-processing of Freeform Optics” project supported by the Korea Basic Science Institute. We thank the support of the Optical Engineering and Fabrication Facility at the University of Arizona. We also thank Bill Anderson for his assistance and his performance of many polishing experiments.

REFERENCES

- J. C. Stover, *Optical Scattering, Measurement and Analysis*, 2nd ed. (SPIE, 1995).
- J. E. Harvey, N. Choi, A. Krywonos, and J. G. Marcen, “Calculating BRDFs from surface PSDs for moderately rough surfaces,” *Proc. SPIE* **7426**, 74260I (2009).
- R. E. Parks, “Specifications: figure and finish are not enough,” *Proc. SPIE* **7071**, 70710B (2008).
- M. J. Cumbo, D. Fairhurst, S. D. Jacobs, and B. E. Puchebner, “Slurry particle size evolution during the polishing of optical glass,” *Appl. Opt.* **34**, 3743–3755 (1995).
- T. Kasai, K. Horio, and A. Kobayashi, “Improvement of conventional polishing conditions for obtaining super smooth surfaces of glass and metal works,” *CIRP Ann.* **39**, 321–324 (1990).
- D. W. Kim and J. H. Burge, “Rigid conformal polishing tool using non-linear visco-elastic effect,” *Opt. Express* **18**, 2242–2257 (2010).
- H. Lei and J. Luo, “CMP of hard disk substrate using a colloidal SiO_2 slurry: preliminary experimental investigation,” *Wear* **257**, 461–470 (2004).
- J. S. Taylor, M. A. Piscotty, N. Q. Nguyen, C. S. Landram, and L. C. Ng, “Efficient polishing of aspheric optics,” Report UCRL-127008 (Lawrence Livermore National Laboratory, 1977).
- J. L. Yuan, P. Zhao, J. Ruan, Z. X. Cao, W. H. Zhao, and T. Xing, “Lapping and polishing process for obtaining super-smooth surfaces of quartz crystal,” *J. Mater. Process. Technol.* **138**, 116–119 (2003).
- G. Zhan, Z. Shen, B. Ma, X. Wang, Z. Wang, H. Liu, and Y. Ji, “Fabrication of supersmooth optical elements with low surface and subsurface damage,” *Proc. SPIE* **8416**, 84162Q (2012).
- Y. Jin, Y. Tong, L. Jiao, D. Wu, and W. Guo, “Influences of grinding and polishing parameters on the quality of super smooth surface,” *Proc. SPIE* **9281**, 92810R (2014).
- X. Nie, S. Li, C. Song, and H. Hu, “Combined fabrication process for high-precision aspheric surface based on smoothing polishing and magnetorheological finishing,” *Proc. SPIE* **9281**, 928111 (2014).
- J. Cao, C. Wei, S. Liu, A. Dun, M. Yang, X. Xu, and J. Shao, “Polishing performances of different optics with different size powder and different pH value slurries during CMP polishing,” *Proc. SPIE* **9633**, 96332O (2015).
- J. Polak, E. Klepetková, J. Pošmourný, M. Šulc, F. Procháska, D. Tomka, O. Matoušek, I. Poláková, and E. Šubert, “Super-polishing of Zerodur aspheres by means of conventional polishing technology,” *Proc. SPIE* **9442**, 944212 (2015).
- T. Döhring, R. Jedamzik, T. Westerhoff, and P. Hartmann, “Four decades of ZERODUR mirror substrates for astronomy,” *Proc. SPIE* **7281**, 728103 (2009).
- P. Hartmann, K. Nattermann, T. Döhring, R. Jedamzik, M. Kuhr, P. Thomas, G. Kling, and S. Lucarelli, “ZERODUR® glass ceramics for high stress applications,” *Proc. SPIE* **7425**, 74250M (2009).

17. T. Hull, A. Clarkson, G. Gardopee, R. Jedamzik, A. Leys, J. Pepi, F. Piché, M. Schäfer, V. Seibert, A. Thomas, T. Werner, and T. Westerhoff, "Game-changing approaches to affordable advanced lightweight mirrors: extreme Zerodur lightweighting and relief from the classical polishing parameter constraint," *Proc. SPIE* **8125**, 81250U (2011).
18. F. W. Preston, "The theory and design of plate glass polishing machines," *J. Soc. Glass Technol.* **11**, 214–256 (1927).
19. N. J. Brown, "Optical polishing pitch," Report UCRL-80301 (Lawrence Livermore National Laboratory, 1977).
20. B. E. Gillman and F. Tinker, "Fun facts about pitch and the pitfalls of ignorance," *Proc. SPIE* **3782**, 72–79 (1999).
21. H. Eyring, "Viscosity, plasticity, and diffusion as examples of absolute reaction rates," *J. Chem. Phys.* **4**, 283–291 (1936).
22. L. M. Cook, "Chemical processes in glass polishing," *J. Non-Cryst. Solids* **120**, 152–171 (1990).
23. T. Izumitani and S. Harada, "Polishing mechanism of optical glasses," *Glass Technol.* **12**, 131–135 (1971).
24. A. Kaller, "Properties of polishing media for polishing optics," *Glass Sci. Technol.* **71**, 174–183 (1998).
25. N. J. Brown, P. C. Baker, and R. T. Maney, "Optical polishing of metals," *Proc. SPIE* **306**, 42–57 (1981).
26. T. Suratwala, R. Steele, M. D. Feit, L. Wong, P. Miller, J. Menapace, and P. Davis, "Effect of rogue particles on the sub-surface damage of fused silica during grinding/polishing," *J. Non-Cryst. Solids* **354**, 2023–2037 (2008).
27. J. B. Johnson, D. W. Kim, R. E. Parks, and J. H. Burge, "New approach for pre-polish grinding with low subsurface damage," *Proc. SPIE* **8126**, 81261E (2011).
28. R. E. Parks, "MicroFinish topographer: surface finish metrology for large and small optics," *Proc. SPIE* **8126**, 81260D (2011).
29. W. Cai, D. W. Kim, P. Zhou, R. E. Parks, and J. H. Burge, "Interferometer calibration using the random ball test," in *International Optical Design Conference and Optical Fabrication and Testing*, OSA Technical Digest (CD) (Optical Society of America, 2010), paper OMA7.
30. J. H. Burge, D. W. Kim, and H. M. Martin, "Process optimization for polishing large aspheric mirrors," *Proc. SPIE* **9151**, 91512R (2014).
31. J. Del Hoyo, D. W. Kim, and J. H. Burge, "Super-smooth optical fabrication controlling high-spatial frequency surface irregularity," *Proc. SPIE* **8838**, 88380T (2013).
32. Universal Photonics Incorporated, Technical Data, <http://universalphotonics.com/Products/Consumables/tabid/102/prtype/1100/Default.aspx>.
33. D. D. Walker, G. Yu, M. Bibby, C. Dunn, H. Li, H. Y. Wu, X. Zheng, and P. Zhang, "Robotic automation in computer controlled polishing," *J. Eur. Opt. Soc.* **11**, 16005 (2016).